Hysteresis Heat Generation in Adiabatic Demagnetization Refrigerator Magnets

P.J. Shirron, M.O. Kimball, and R.S. Ottens

NASA/Goddard Space Flight Center
Greenbelt, MD 20771

ABSTRACT

Adiabatic demagnetization refrigerators (ADR) are increasingly being used as an auxiliary cooling system with mechanical cryocoolers, to achieve lower operating temperature or to improve efficiency. One recent development is multi-staging[1] that enables continuous operation at temperatures well below 1 K using a 4 K-class GM, pulse tube, or Joule-Thomson cryocooler. Continuous operation involves cyclic magnetization and demagnetization of the refrigerant on short time scales – from 10s of minutes to 10s of seconds. This is achieved by charging and discharging a superconducting magnet over field excursions of up to a few tesla. The hysteresis heat generated can be a significant fraction of the total heat rejected during operation, and therefore can significantly reduce efficiency. Recent measurements of hysteresis heat generation have been made at NASA/GSFC using multifilamentary NbTi magnets produced for the Resolve instrument on the X-Ray Imaging and Spectroscopy Mission (XRISM)[2]. Results of these measurements and a mathematical analysis method for extracting instantaneous heating rates are presented.

INTRODUCTION

Hysteresis heat is generated within superconducting magnets due to magnetic flux penetration into the superconductor and eddy currents within the normal metal stabilizer[3]. For ADRs, the heat produced by cyclic charging and discharging during a cooling cycle is typically comparable to the heat rejected from the salt pill, and therefore can represent a significant reduction in efficiency. In continuous ADRs that are cycled rapidly, the instantaneous heating rate can be problematic for several reasons. First, it imposes a heat load on the heat sink, and ADRs using low power space cryocoolers may require controlling ramps rates in order to remain within the available cooling power. Second, it raises the internal magnet temperature, which for higher temperature applications (NbTi magnets at $\geq$5 K) may also require controlling ramp rates to avoid exceeding the magnet's critical temperature.

It is therefore useful at early stages of design and system optimization to estimate instantaneous heating rates in ADR magnets. Direct measurement is complicated by internal and external time constants of the magnet and its connection to its heat sink, especially when a ferromagnetic shield is present. That is, heat generated in the magnet distributes within the

Cryocoolers 21, edited by R.G. Ross, Jr., J.R. Raab and S.D. Miller

magnet and flows out to the heat sink at characteristic times that can range from tens of seconds to minutes. Since ramp durations are also the same order of magnitude, temperatures within the system are not simply related (i.e. proportional) to the instantaneous heating rate. Nevertheless, a straightforward iterative analysis method allows the instantaneous heat generation rate to be extracted from a set of magnet temperatures, with some additional knowledge of physical parameters such as the thermal conductance between the locations where the magnet and base temperatures are measured.

Measurements of hysteresis can be made *in situ* for most applications with the simple addition of a thermometer and heater for calibration of thermal conductance. For this work, we assembled a dedicated apparatus in which a magnet and shield (if included) was supported by an aluminum standoff from an aluminum cold plate. The magnet mandrel, standoff and cold plate were instrumented with thermometers and heaters. The heaters were used both for measuring thermal conductance and to temperature-control various components so that total heat flow during a ramp could be measured; this served as a check on the analysis method that the instantaneous hysteresis heating rate integrates to the total measured flow.

Dedicated measurements were made with the CPA-stage magnet built for the Resolve instrument on XRISM. Measurements with and without its magnetic shield, combined with modeling of the magnetic field within the windings, indicate that the increase in hysteresis heating with the shield present is entirely due to the enhanced magnetic field within the winding pack, and not from heating within the shield. Other measurements of both the CPA-stage and GLF-stage magnets during operation of the Resolve ADR are used to test the utility of scaling rules developed from the theoretical dependence of hysteresis heating on the physical properties of the NbTi wire and structure of the magnets. Design and performance details are provided in Table 1.

ANALYSIS METHOD AND CALIBRATION

For purposes of this analysis, the magnet and shield (if present) are treated as a lumped heat capacity, C, connected to a heat sink through a thermal conductance K. This system is characterized by a time constant $\tau = C/K$. In practice, there may be background heat loads or calibration biases which cause the magnet's steady state temperature, Tss, in the absence of any other heating, to be different than the sink. The analysis relies on temperature changes relative to T_{SS}.

It is assumed that a set of temperatures, $T_m(t_i)$, has been obtained during the application of heat or a magnet ramp. The goal is to derive the set of heat loads, $\dot{Q}(t_i)$, that would produce the measured temperatures. The process is iterative, where an initial estimate of heat loads is used to calculate the temperature response, and the heat loads are refined based on the difference between the calculated and measured response.

Table 1. Design and performance parameters for the Resolve ADR magnets

	CPA-stage Magnet	GLF-stage Magnet
Central field	2 T at 2 A	3 T at 2 A
Average field in bore (with magnetic shield)	0.91 T/A	1.46 T/A
Average field in bore (without magnetic shield)	0.84 T/A	1.36 T/A
Wire type (Supercon, Inc., type 15S40)	15 filament NbTi, 1.4:1 Cu:NbTi ratio, 0.075 mm diameter bare wire, 0.1 mm coated	
Winding dimensions (cm)	ID=4.61, OD=6.40, L=13.7	ID=2.73, OD=5.58, L=8.10
Number of turns	107320	111820
Length of wire (km)	18.54	14.60
Volume of windings (cm^3)	213.0	150.7
Volume of NbTi (cm^3)	37.5	28.3
Inductance (H)	220	200

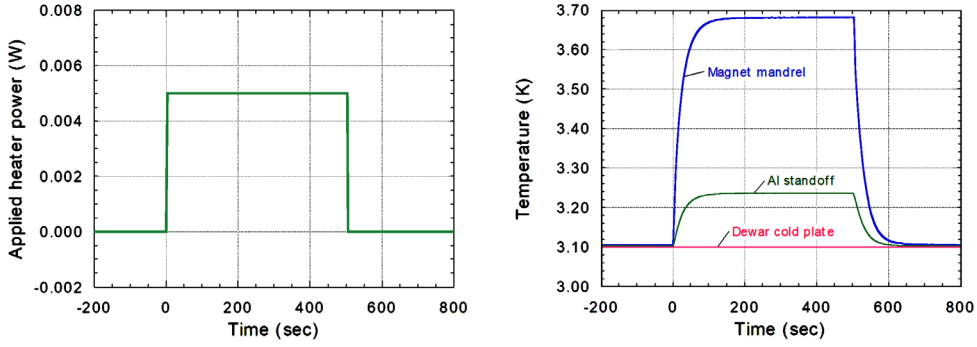

Figure 1. Plots of the applied heat load (left), and temperature responses (right).

The basis of the calculation is that in each time interval, $t_{i-1} \rightarrow t_i$, temperature will change as an exponential approach to an equilibrium value, $T_{eq}(t_i) = T_{SS} + \dot{Q}(t_i)/K$. Over each measurement interval, the temperature changes according to

$$T_{m,exp}(t_i) = T_{m,exp}(t_{i-1}) + \left(T_{eq}(t_i) - T_{m,exp}(t_{i-1})\right)\left(1 - e^{-(t_i - t_{i-1})/\tau}\right) \quad (1)$$

with

$$T_{m,exp}(t_0) = T_{eq}(t_0). \quad (2)$$

Heat loads are then revised as

$$\dot{Q}'(t_i) = \dot{Q}(t_i) + K \bullet \left(T_m(t_i) - T_{m,exp}(t_i)\right). \quad (3)$$

A new set of temperatures is calculated, and the iteration continues until heat loads and temperatures stabilize. In practice, any initial set of $\dot{Q}(t_i)$ will eventually stabilize at the same final values, but to save some computation, a suitable starting point is $\dot{Q}(t_i) = K \bullet (T_m(t_i) - T_{SS})$.

Physical Constants

This analysis depends on independently determining values for K, τ, and T_{SS}, and there are various methods available. T_{SS} is simply the steady state temperature with no applied heat, and K can be measured by applying a heat load to the magnet or the aluminum standoff and measuring the temperature rise relative to T_{SS}. τ is easily determined by fitting to an exponential decay a portion of the dataset where the temperature starts off elevated and relaxes to its asymptotic value (T_{SS}) in the absence of any heat load. In practice, any instance where there is a step change in heat load can be used to determine τ.

Calibration

A first test of the analysis method is whether it can reproduce a known heat pulse, such as that used to calibrate the thermal conductance. This was typically the application of a 5 mW heat load to the magnet mandrel for 500 seconds. The applied load and temperature response of the mandrel and at the Al standoff are shown in Fig. 1 for a test of the magnet without magnetic shield. The exponential fit of temperatures after the heater was turned off to exponential decays gives time constants of 25.81 s and 25.98 s for the mandrel and standoff responses, and the steady state temperature differences gave thermal conductances of 8.67 mW/K and 35.7 mW/K,

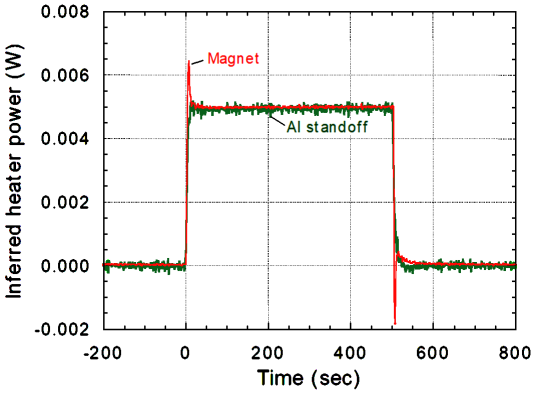

Figure 2. Heat pulse inferred from the magnet mandrel and Al standoff temperature responses.

respectively. For both temperature sets, the steady state temperature was 3.107 K. (Time constants with a magnetic shield installed were on the order of 108 s.)

Using these parameters, the heat loads inferred from both temperature responses, shown in Fig. 2, closely approximate the actual load in both magnitude and time dependence. There are, however, some discrepancies, and their origin is important to understand as they can point to potential improvements in experiment design and data collection. Most important, the time interval between temperature measurements (~2 s) and their timing relative to the start and end of the heat pulse impose limits on the ability to reconstruct a very sharp heat pulse. This is evident in the over- and undershoot of heater power at the transitions. More frequently spaced measurements can improve the resolution in this regard, but it can also significantly degrade resolution of steady heat loads, as temperature noise (i.e. apparent temperature changes over very short time scales) translates to large heat load fluctuations. The second notable feature is a longer term (tens of seconds) decay of the heat load to a steady state value (5 mW or zero). This suggests that the experimental system may have multiple time constants. In this case, the mandrel connects to separate masses – the windings and the standoff – and likely has different time constants for heat transfer.

A final observation is that while the larger temperature response of the mandrel yields better resolution of the heat load, the combined effects of limited data rate and possible multiple time constants results in poorer resolution of rapid changes in heat load.

HYSTERESIS MEASUREMENTS

A full ADR cycle involves a ramp of the magnet current from zero to a peak value and back to zero. For these measurements, each ramp consisted of 1) a hold at zero current, 2) a linear ramp from zero to peak current (usually 2.0 A), 3) hold at peak current, and 4) a linear ramp to zero. Ramp rates were varied from 1.25 mA/sec to 5 mA/sec, corresponding to voltages at the windings of 0.25 to 1.0 V. The goal was to assess any rate dependence, which would suggest eddy current heating in the magnet or shield. No such dependence was identified.

Fig. 3 shows the typical time dependence of the current, temperature response at the Al standoff, and the inferred instantaneous heating rate. The heating rate is normalized by the magnet voltage. As before, some undershoot in the inferred heating rate is observed at abrupt changes in heat load, such as when the current stops at zero or 2 A.

Overshoots at the beginning of a ramp are not observed because the heating rate does not, in fact, change abruptly. This can be seen when the heating rate is plotted as a function of current, as in Fig. 4. Here the heating rate for repeated 2 A cycles is compared to the rate obtained from a steady ramp from >2.5 A to zero. The arrows matching the color of the two data sets show the direction of current ramping.

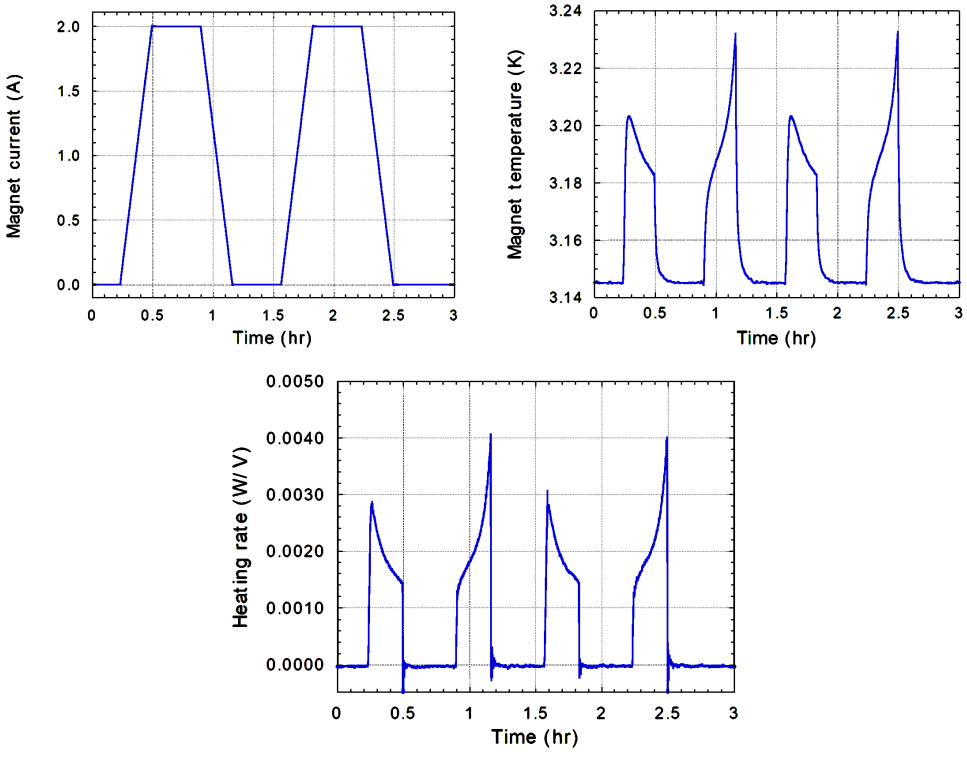

Figure 3. Heat pulse inferred from the magnet mandrel and Al standoff temperature responses.

Based on measurements for a variety of ramp parameters (for example 0->2A->0, 0->1A->0, 1A->2A->1A), the analysis supports the following general conclusions:

1. Hysteresis heat generation drops to zero when magnet current reverses direction, and increases back to its nominal value over an excursion in current.
2. The excursion is different for increasing and decreasing currents, but does not depend on the value of current at which the reversal occurs.
3. The nominal heating rate (i.e. after the current changes beyond the characteristic value) is the same for increasing and decreasing currents.

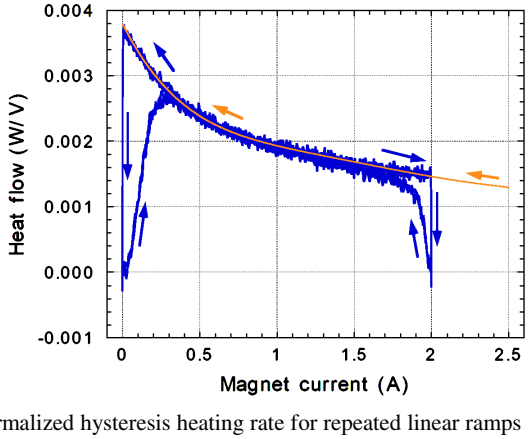

Figure 4. Normalized hysteresis heating rate for repeated linear ramps to 2 A compared to a single descending ramp from 2.5 A to zero. Arrows indicate the direction of current change.

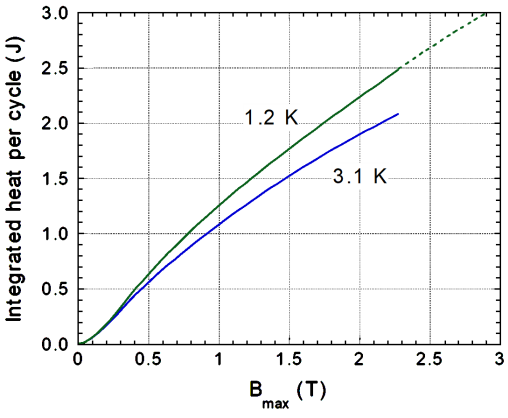

Figure 5. Integrated heat generated within the Resolve CPA-stage magnet and shield for a cycle from zero to B_{max} to zero. Measurements at 1.2 K have been extrapolated to higher field (dotted line) to enable scaling to higher field magnets.

In addition, measurements at different temperatures show a more modest dependence than would be expected from the typical change in the critical current of NbTi wire as suggested in [Bottura], as discussed in the next section. Figure 5 shows the integrated value of hysteresis heat for a complete current cycle from zero to B_{max} to zero, for measurements at 1.2 K and 3.1 K. For this figure, magnet current has been scaled by the average field to current ratio listed in Table 1.

SCALING RULES

One of the goals of this study was to develop scaling rules for extrapolating hysteresis measurements for one magnet to another. To do so, it is necessary to identify how hysteresis heating depends on both the material properties of the superconducting wire and on the geometry of the magnet.

Using the formulation in [Wilson], the heat generated in a unit volume of superconductor when the magnetic field increases from zero to B is

$$q(B,T) = \frac{8}{3\pi} a \int_0^B j_c(B,T) dB \qquad (4)$$

where a is the radius of the NbTi filament(s) in the wire and $j_c(B,T)$ is the critical current density of the NbTi filaments as a function of field and temperature. To calculate the heat generated in a magnet (for a ramp from zero to some current), $q(B,T) \cdot f$ is integrated over the volume of the windings, where B is the field in each volume element at current, and f is the volume fraction of NbTi superconductor in the windings.

The double integral intertwines the superconducting properties with magnet geometry in a way that makes it difficult to develop scaling rules that apply over a wide range of magnetic fields and magnet structure, especially when magnetic shielding (e.g. ferromagnetic, superconducting or active coils) are included. Nevertheless, this formulation does give some insight into relative importance of various parameters.

The obvious dependences are that hysteresis heat is proportional to 1) the NbTi filament radius, 2) the critical current density, and 3) the volume of NbTi in a magnet. The latter is the product of the volume fraction of NbTi in the wire and the volume fraction of wire in the winding pack. Less obvious is that, for simple solenoids where the average field in the bore is , the field within the windings is roughly a linear distribution such that every field value between zero and occupies equal volume. The extent to which this is true depends on aspect ratio and magnetic shielding, but it otherwise suggests that the curves in Fig. 5 can be used to scale between magnets having different field to current ratios. That is, two magnets using the same amount of wire but having different turns/meter will produce different fields, but the relative hysteresis heat generated for a full cycle can be read of the curve for the appropriate temperature in Fig. 5.

Table 2. Comparison of measured and scaled hysteresis totals for Resolve magnets

	Measured hysteresis heat for 2 A cycle (J)	Avg bore field at 2 A (T)	Scale factor for NbTi volume	Scaled hysteresis heat (J)
CPA-stage magnet, shielded	2.073	1.82		
CPA-stage magnet, no shield	1.930	1.67	1	1.95
GLF-stage magnet, shielded	1.830	2.90	0.755	2.11

One final scaling rule comes from [Bottura], which finds that $j_c(B,T)$ can be separated as $j_c(B)g(T)$, where $g(T) = (1-(T/T_c)^{1.7})^{\gamma}$ and γ is typically in the range of 1.8-2.1. As a result, hysteresis measurements can simply be scaled by $g(T)$ to account for different operating temperatures. The scale factor for the data in Fig. 5 would be $g(1.2)/g(3.1)$~1.3, while the apparent ratio is only about 1.2.

Application of scaling rules to XRISM magnets

As a limited check of these scaling rules, we compare the hysteresis heat generated by the two Resolve magnets. Two test cases are available: scaling between shielded and unshielded CPA-stage magnet, and between CPA-stage and GLF-stage magnets. Table 2 gives the measured hysteresis heat for full cycles to 2 A, compared to scaled values obtained from Fig. 5 and adjusting for the volume of NbTi. There is good agreement for the shielded and unshielded CPA-stage magnets, while the scaling significantly overestimates heating in the shielded GLF-stage magnet. By evaluating the field distribution in the windings, we find that the addition of ferromagnetic shielding uniformly enhances the field without significant change in spatial pattern, while the smaller aspect ratio of the GLF-stage magnet increases the fractional volume which experiences mid-level fields (half of peak) and reduces the fractional volume that experiences the highest fields. Skewing the volume distribution toward smaller fields should result in lower hysteresis losses.

CONCLUSIONS

Hysteresis heating in superconducting magnets can be a significant factor in the design of ADRs, especially for space instruments where thermal and power budgets are limited and systems must be designed as closely as possible to match cooling powers with heat flows. Typically hysteresis is measured over round-trip magnetic field excursions to yield a time average heating rate, but in some cases it is necessary to know – and control – the instantaneous rate. We have made measurements of hysteresis for two magnets with different aspect ratios and field to current ratios that were built for the Resolve instrument on XRISM, and have developed an analysis method for recovering instantaneous heating rates from a magnet's temperature response. Those rates can be integrated to yield total heating over any change in field. Among the findings is that for the Resolve instrument, hysteresis heat is approximately 40% of the total heat rejected over an ADR cycle. We also observe that hysteresis heating has the same dependence on magnet current for positive and negative ramp rates, but is suppressed over a characteristic excursion in magnetic field when the ramp direction is reversed.

To facilitate extrapolation of these results to other magnets, we present scaling rules based on the dependence of hysteresis heating on the properties of NbTi and the magnet wire, and field distribution in the windings. Although this study involved measurements for only a few magnet configurations, the agreement between measured and scaled heating rates is best among magnets with similar spatial distribution of magnetic field in the windings. That is, the uncertainty in scaling increases with differences in aspect ratio and structures that alert the field pattern such as active shield coils.

REFERENCES

1. Shirron P.J., Abbondante N., Canavan E.R., DiPirro M.J., Grabowski M., Hirsch M., Jackson M., Panek J., Tuttle J.G., "A Continuous Adiabatic Demagnetization Refrigerator for Use with Mechanical Coolers," *Cryocoolers 11,* Kluwer Academic/Plenum Publishers, New York (2001), pp. 587-96.

2. Shirron, P.J., et al., "Design and On-orbit Operation of the Soft X-ray Spectrometer Adiabatic Demagnetization Refrigerator on the Hitomi Observatory," *J. Astron. Telesc. Instrum. Syst*. 4(2), 021403 (2018).

3. Wilson, M.N., *Superconducting Magnets*, Oxford Science Publications, Oxford (1983), pp. 159-184.

4. Bottura, L., "A Practical Fit for the Critical Surface of NbTi," *IEEE Transactions on Applied Superconductivity*, vol. 10, no. 1 (2000), pp. 1054-1057.